ChemistrySelect

Research Article
doi.org/10.1002/slct.202104338

Chemistry Europe
European Chemical Societies Publishing

www.chemistryselect.org

Electro, Physical & Theoretical Chemistry

Quantitative Investigation of Halogen and Hydrogen Bonding in 2-Chloro, 4-X-Benzoic Acids

G. N. Anil Kumar[b] and Venkatesha R. Hathwar*[a]

Dedicated to Prof. T. N. Guru Row on the occasion of his 70th birthday.

The crystal structure, Hirshfeldsurface analysis, topological analysis of the electron density and total interaction energies of four compounds, 2-Chloro, 4-X-Benzoic Acids (where X = I, Br, Cl and F) have been analysed. The packing similarity was evaluated in all compounds using the *XPac* analysis. The qualitative information about intermolecular interactions is derived from the crystal structure and Hirshfeld surface analyses whereas quantitative information are determined by the QTAIM analysis as well as total interaction energies from *CrystalExplorer*. The topological properties are estimated for all compounds in both crystal geometry and gas phase using *TOPOND* and *AIMALL*, respectively. The carboxylic acid O–H···O HB dimers, C–H···O HBs and $C_\pi\cdots C_\pi$ aromatic stacking interactions are found to be common interactions in all compounds. The topological properties and bond paths demonstrate them as non-covalent stabilizing interactions in the crystalline state. The hierarchy of interactions concerning their strength is observed in the following order such that O–H···O HB dimers > $C_\pi\cdots C_\pi$ aromatic stacking interactions > C–H···O HBs > Type II X···Cl interactions and C–H···Cl HBs > Type I homo-halogen X···X interactions in all compounds. Additionally, the strength of Type I homo-halogen X···X interactions vary in the order: I···I > Br···Br > Cl···Cl > F···F. The hierarchy of interactions is further supported by molecular electrostatic potential surfaces associated with both positive and negative potential regions.

Introduction

Non-covalent interactions such as hydrogen bonding (HB) and halogen bonding (XB) play a significant role in crystal engineering[1] and supramolecular chemistry.[2,3] Similar to HB, XB has become a driving force in polymorphism[4], anion transport,[5] phosphorescence,[6] gelation,[7] solar cells,[8] drugs discovery[9] and in many biological systems.[10] Several reviews highlight the significant contributions of XB in materials and biological sciences.[11–16] Halogen (X) atom in the XB acts as both Lewis acid and Lewis base due to the formation of σ-hole along the axis of the R–X covalent bond.[17] In XB, the X atom is an acceptor of electron density from the Lewis base. Hence, XBs are directional and attractive interactions. The positive electrostatic potential is formed along the R–X bond is referred to as σ-hole by Politzer.[18] The origin of such positive potentials is described by a half-filled *p* orbital on the covalently bonded halogen atom, which creates an electron deficient region in the outer lobe of the *p* orbital. Thus, the subsequent electrostatic attractive interactions by the participation of σ-hole in supramolecular assembly are also known as σ-hole bonding.[19] The C–X···X–C interactions in the solid-state are extensively explored in the literature and characterized using three geometrical parameters, R_{ij} = X···X, two angles θ_1 = R–X···X and θ_2 = X···X–R. The interactions with $\theta_1 \cong \theta_2$ are known as type I (includes both *cis* and *trans* geometry) interactions, whereas interactions with $\theta_1 \cong 180°$ and $\theta_2 \cong 90°$ are referred to as type II (*L-geometry*) interactions.[20,21] Indeed, the type-II X···X interactions are considered as XB and they are considered as an attractive interaction.[22] The attractive, directional and stabilizing nature of type-II X···X interactions are experimentally established by high-resolution electron density studies.[21,23,24] In later years, the participation of F atom in X···X interactions is also demonstrated using both experimental and theoretical studies.[25–28] The strength of the XB depends on a participating X atom in the XB and it follows the extend of the σ-hole formation on the halogen atom. Further, the cooperativity between HB and XB is well documented in recent reviews and studies.[29–31] It has been shown in selenourea that the presence of HB enhances the formation of XB in the crystal structure,[32] Similarly, increased thermal stability and activity of the enzyme at elevated temperatures is observed in *m*-chlorotyrosine due to the cooperative effects of HBs and XBs.[33] Thus, both HB and XB play an important role in structural stability and subsequent properties.

The analysis of electron density distribution based on Bader's 'quantum theory of atoms in molecules' (QTAIM)[34] approach is popular to quantify the intermolecular interactions

[a] *Dr. V. R. Hathwar*
School of Physical and Applied Sciences
Goa University
Taleigao Plateau 403206, India
E-mail: vhathwar@unigoa.ac.in
[b] *Dr. G. N. Anil Kumar*
Department of Physics
M. S. Ramaiah Institute of Technology
Bangalore, Goa 500054, India

Supporting information for this article is available on the WWW under https://doi.org/10.1002/slct.202104338

in the molecular crystals. The topological properties of the electron density are used to classify intermolecular interactions into strong and weak interactions.[35] It is a quantitative evaluation of interactions and provides additional information over the qualitative description using the bond lengths and bond angles[36,37]. Further, the Hirshfeld surface is determined by the density weight function of the pro-molecule over the pro-crystal, thus resulting in isosurfaces, which account effects of neighbouring molecules in the crystal.[38] Hence, the HS provides information about various intermolecular interactions found in the crystalline state. It can be determined over different properties namely, d_{norm}, electrostatic potential, shape-index and curvedness. Recently, the strength of intermolecular interactions in the crystalline state could be accessed by the HS using *CrystalExplorer*.[39] Indeed, an individual contribution to intermolecular interactions such as Coulombic, polarization, dispersion and repulsion components could be determined for all interactions in the crystal geometry. They provide insights on the hierarchy of different interactions based on their energies. Indeed, quantitative information is necessary to evaluate their role in the crystal packing and stabilization of the crystal structure.

In the present paper, we have explored hetero-halogen X···Cl and homo-halogen X···X (X: I, Br, Cl, F) interactions in the presence of carboxylic acid O–H···O HB dimers in 2-chloro, 4-X-benzoic acids based on the QTAIM analysis and interaction energies. The systematic studies of topological properties and interaction energies of X···Cl interactions involving different halogens in similar compounds are sparse in the literature. Thus, the role of HBs and XBs in dictating the packing of molecules and stabilization of crystal structures has been discussed. The schematic diagram of compounds used in the present study, 2-chloro, 4-iodo-benzoic acid (**1**), 2-chloro, 4-bromo-benzoic acid (**2**), 2-chloro, 4-chloro-benzoic acid (**3**) and 2-chloro, 4-fluoro-benzoic acid (**4**) is shown in Scheme 1.

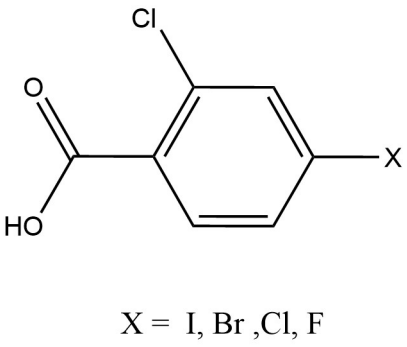

Scheme 1. Schematic diagram of 2-chloro, 4-X-benzoic acids explored in the present study.

Results and Discussion

Crystal Structure and Hrishfeld Surface (HS) Analysis

ORTEP diagrams of compounds **1**–**4** are shown in Figure 1. The crystallographic and structural refinement details are listed in Table 1. The crystal structures of **2**[40,41] and **4**[25] were already reported in the literature whereas the crystal structures of **1** and **3** were determined for the first time. However, it is interesting to note that cocrystals of **3** with different coformers such as 4-amino-5-chloro-2,6-dimethylpyrimidine[42] and *L*-proline[43] were known. The compounds **1** and **2** have isomorpous structures and crystallize in the monoclinic, $P2_1/n$ space group with Z = 4 (Table 1). The common intermolecular interactions in the crystal packing are the carboxylic acid O–H···O dimers, C–H···O HBs and C_π···C_π aromatic stacking interactions (Figure S1 and Table 2). Additionally, both structures are stabilized by type-I homo-halogen X···X and type-II hetero-halogen X···Cl interactions (where X = I and Br for **1** and **2**, respectively). It is observed that the cooperative participation of type I homo-halogen X···X and type II hetero-halogen X···Cl interactions in the crystal packing has resulted in X_3 synthon. Further, the C–H···Cl HBs and X···C_π interactions are found in both structures. Similarly, compounds **3** and **4** depict isomorpous structures in the triclinic P-1 space group with Z = 2 (Table 1). The major intermolecular interactions in the packing are the carboxylic acid O–H···O dimers, C–H···O and C–H···Cl HBs and C_π···C_π aromatic stacking interactions (Figure S1 and Table 2). The distinct packing features between two structures are C–H···Cl dimer, type-I and type-II homo-halogen Cl···Cl interactions for **3** whereas C–H···F dimer and type-II hetero-halogen F···Cl interactions for **4** (Table 2). It is interesting to note that the type-I homo-halogen F···F interaction is not observed in **4** and the C–H···F dimers are preferred over the F···F interaction. The percentage contributions of different interactions are highlighted in a fingerprint plot of the HS analysis in Figure 2. The HS analysis further validates the isomorphous features between **1** and **2**, as well as between **3** and **4**. Further, the HS obtained by mapping d_{norm}, shape-index

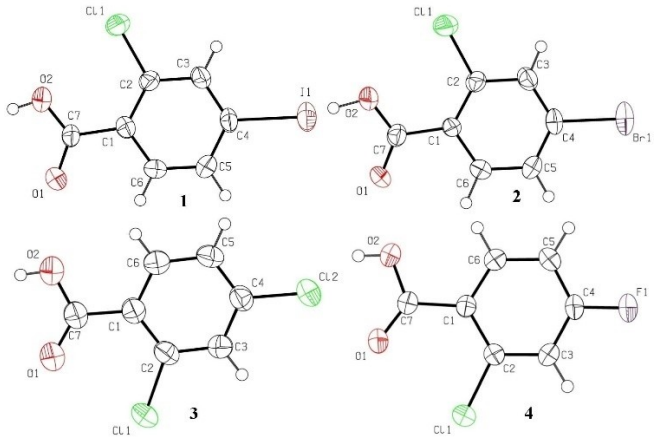

Figure 1. *ORTEP* plots of compounds **1**–**4** with displacement ellipsoids drawn at 50% probability level.

Table 1. Crystallographic and structural details of compounds, **1**–**4**.

Crystal data	1	2	3	4
Chemical formula	$C_7H_4ClIO_2$	$C_7H_4BrClO_2$	$C_7H_4Cl_2O_2$	$C_7H_4ClFO_2$
Molecular weight	282.45	235.46	191.00	174.55
Crystal system,	Monoclinic	Monoclinic	Triclinic	Triclinic
Wavelength (Å)	0.71073	0.71073	0.71073	0.71073
space group	$P2_1/n$	$P2_1/n$	P-1	P-1
a (Å)	7.790 (5)	7.483 (5)	3.8958 (3)	3.82285 (10)
b (Å)	9.265 (5)	9.032 (5)	8.0817 (6)	7.7653 (3)
c (Å)	11.768 (5)	11.859 (5)	12.1568 (10)	12.1888 (5)
α (°)	90	90	91.611 (6)	77.149 (4)
β (°)	101.166 (5)	103.309 (5)	91.009 (6)	83.961 (3)
γ (°)	90	90	101.564 (7)	76.479 (3)
V (Å^3)	833.3 (8)	780.0 (8)	374.73 (5)	342.45 (2)
Z	4	4	2	2
μ (mm^{-1})	4.11	5.55	0.80	0.51
Crystal size (mm)	0.32×0.30×0.25	0.35×0.30×0.30	0.32×0.21×0.12	0.35×0.25×0.21
T_{min}, T_{max}	0.353, 0.427	0.247, 0.287	0.783, 0.910	0.861, 0.900
Measured reflections	8747	8250	7412	8137
Unique reflections	1642	1539	1462	1345
Observed - reflections [$I > 2\sigma(I)$]	1219	984	1163	1077
R_{int}	0.040	0.052	0.061	0.032
$(\sin\theta/\lambda)_{max}$ (Å^{-1})	0.617	0.617	0.617	0.616
$R[F^2 > 2\sigma(F^2)]$, $wR(F^2)$, S	0.027, 0.089, 0.62	0.029, 0.049, 0.84	0.070, 0.239, 1.16	0.033, 0.087, 1.04
No. of reflections	1642	1539	1462	1345
No. of parameters	101	116	95	101
H-atom treatment	constrained	constrained	constrained	constrained
$\Delta\rho_{max}$, $\Delta\rho_{min}$ (e Å^{-3})	0.30, −0.66	0.29, −0.43	0.67, −0.38	0.26, −0.24
CCDC numbers	2069046	2069043	2069044	2069045

and curvedness properties is shown in the supporting information (Figure S2). The HS analysis highlights the contribution of both strong and weak interactions in the crystal lattice. The cooperative effects between HBs and XBs dictate the stability of the crystal structures. The strength of these interactions is evaluated using the QTAIM analysis and Hirshfeld surfaces are discussed in the later section.

Packing similarity analysis

The packing similarity was evaluated using the *XPac* program.[44] The similarities in supra-molecular features of different crystal structures in 3D, 2D, 1D and 0D are identified and obtained results are listed in Table 3. The study suggests **1** versus **2** show 3D similarity but it has the lowest degree of dissimilarity index 2.3 when compared with other pairs of crystal structures such as **3** and **4**. The structures **2** and **3** as well as **2** and **4** show 0D similarity with a high dissimilarity index of 4.0 and 3.5, respectively. The crystal structures **3** and **4** show 2D similarity with dissimilarity index 2.6. The 0D illustrates the presence of different packing motifs in the crystal structures. The comparison of molecular packing for structures **1**–**4** was also estimated using the *CrystalCMP* program.[45] The dendrograms were calculated from a similarity matrix using the unweighted pair group method with arithmetic mean (UPGMA). The dendrogram with green and red colors indicates dissimilar and similar packing between crystal structures. The green color for **1** vs **2** and **3** vs **4** indicates almost similar packing between them as depicted in Figure 3. Further, the similarity PS_{ab} values for 1 vs 2 and 3 vs 4 are 0.3032 and 0.9241, respectively. The packing analysis supports earlier crystal structure discussions based on iso-structural features in a quantitative way.

Total Energies of Intermolecular Interactions

Quantitative information about energetics of different intermolecular interactions present in the crystal structure is obtained from the Hirshfeld surface[38] in *CrystalExplorer*.[39] The pairwise total energy of interactions is the sum of electrostatic (E_{ele}), polarization (E_{pol}), dispersion (E_{dis}) and exchange repulsion (E_{rep}) terms. The intermolecular interaction energies from B3LYP/6–311G(d,p) and B3LYP/DGDZVP functional are listed in Table 4 and Table S2, respectively. The B3LYP/DGDZVP functional is tested for interactions involving heavier halogens. There are no significant differences in the hierarchy of interaction energies by using the DGDZVP functional. There are many equivalent molecular motifs observed in the crystal packing of **1**–**4** as discussed in section 3.1. The equivalent motifs in all compounds were analysed in terms of total energies and individual components of contributing energies. Among them, the carboxylic acid O–H···O HB dimers, C–H···O HBs and $C_\pi\cdots C_\pi$ aromatic stacking interactions are common interactions in all compounds. The hierarchy of interactions can be arranged in

Table 2. List of intermolecular interactions present in compounds **1**–**4**.

Interactions	Interaction distance d(Å)	Angle θ(°)	Symmetry
1			
I1···I1 (type-I)	3.880(1)	$\theta_1=\theta_2=148.8(1)$	−x+1,−y,−z+2
I1···Cl1 (type-II)	3.797(1)	$\theta_1=162.4$, $\theta_2=90.1(1)$	x-1/2,−y+1/2,+z−1/2
O2–H2···O1	1.686(1)	174.1(1)	−x+2,−y+2,−z+2
C5–H5···O1	2.332(1)	178.4(1)	−x+1/2+1,+y-1/2, −z+1/2+1
C3–H3···Cl1	2.919(1)	149.8(1)	x−1/2,−y+1/2,+z−1/2
C2···C6 (π···π)	3.576(0)	–	−x+2,−y+1,−z+2
I1···C2 (I···π)	3.857(0)	–	−x+1,−y+1,−z+2
2			
Br1···Br1 (type-I)	3.699(1)	$\theta_1=\theta_2=150.9(1)$	−x,−y−1,−z+2
Br1···Cl1 (1) (type-II)	3.703(1)	$\theta_1=146.9(1)$ $\theta_2=115.6(1)$	x-1/2,−y−1/2,+z−1/2
Br1···Cl1 (2) (type-II)	3.799(1)	$\theta_1=161.8(1)$ $\theta_2=91.9(1)$	−x+1/2,+y−1/2, −z+1/2+2
O2–H2···O1	1.694(1)	174.0(1)	−x+2,−y+2,−z+2
C5–H5···O1	2.275(1)	168.8(1)	−x+1/2+1,+y−1/2, −z+1/2+1
C3–H3···Cl1	2.802(1)	149.8(1)	x-1/2,−y−1/2,+z−1/2
C3···C5 (π…π)	3.593(1)	–	−x,−y,−z+2
Br1···C2 (Br…π)	3.754(1)	–	−x,−y,−z+2
3			
Cl1···Cl2 (type-I)	3.695(1)	$\theta_1=127.0(1)$ $\theta_2=122.0(1)$	x+1,+y+1,+z
Cl1···Cl2 (type-II)	3.342(2)	$\theta_1=165.9(1)$ $\theta_2=106.5(1)$	−x,−y+1,−z
O2–H2···O1	1.682(1)	169.0(1)	−x+2,−y+1,−z+1
C5–H5···O1	2.862(1)	168.7(1)	x,+y−1,+z
C3–H3···Cl2	2.931(1)	154.5(1)	−x,−y,−z
C6–H6···O2	2.865(1)	138.8(1)	−x+2,−y,−z+1
C4···C5 (π…π)	3.491(1)	–	x−1,+y,+z
C1···C2 (π…π)	3.487(1)	–	x+1,+y,+z
4			
Cl1···F1 (type-II)	3.066(1)	$\theta_1=170.3(0)$ $\theta_2=116.5(1)$	x,+y−1,+z
O2–H2···O1	1.676(1)	171.3(1)	−x+2,−y+1,−z+1
C5–H5···O1	2.513(1)	164.5(1)	x,+y+1,+z
C3–H3···F1	2.506(1)	137.5(1)	−x,−y+2,−z+2
C6–H6···O2	2.619(1)	138.9(1)	−x+2,−y+2,−z+1
C5–H5···Cl1	2.974(1)	127.1(1)	x,+y+1,+z
C1···C2 (π…π)	3.483(0)	–	x+1,+y,+z

Table 3. The packing similarity was analyzed using the *XPac* program.

Compounds	**1** vs **2**	**1** vs **3**	**1** vs **4**	**2** vs **3**	**2** vs **4**	**3** vs **4**
Dimensionality	3D	0D	0D	0D	0D	2D
Dissimilarity Index (X)	2.3	3.3	2.8	4.0	3.5	2.6
Stretch Parameter (D)Å	0.17	0.01	0.02	0.01	0.02	0.21
Δα (angles,°)	1.2	2.8	1.7	2.4	1.4	1.7
Δρ (planes,°)	1.9	1.8	2.3	3.2	3.3	1.9

the decreasing order according to their strength such that O–H···O HB dimers > C_π···C_π aromatic stacking interactions > C–H···O HBs > Type II X···Cl interactions and C–H···Cl HBs > Type I homo-halogen X···X interactions (Table 4). The carboxylic acid O–H···O HB dimers are the strongest interactions among all and their total energy varies in the range from −74.7 to −84.4 kJmol^{-1}. For O–H···O HB dimers, the electrostatic component is the major contribution (from −139.0 to −143.0 kJmol^{-1}) (Table 4). Figure 4 shows energy frameworks with the electrostatic, dispersion and total interaction energy components for the carboxylic acid O–H···O HB dimers in the form of cylindrical tubes for **1**, **2**, **3** and **4**. In terms of the total energy, the C_π···C_π aromatic interactions are significantly contributing to the stabilization of the crystal structures in all compounds (from −23.4 to −37.6 kJmol^{-1}) where both electrostatic (E_{ele}) and dispersion (E_{dis}) terms are significant contributors to the total energy. In the case of common C–H···O HBs, the total energy varies in the range from −4.1 to −16.2 kJmol^{-1} where the electrostatic (E_{ele}) and dispersion (E_{dis}) terms are equally contributing to the total energy. It is interesting to note that

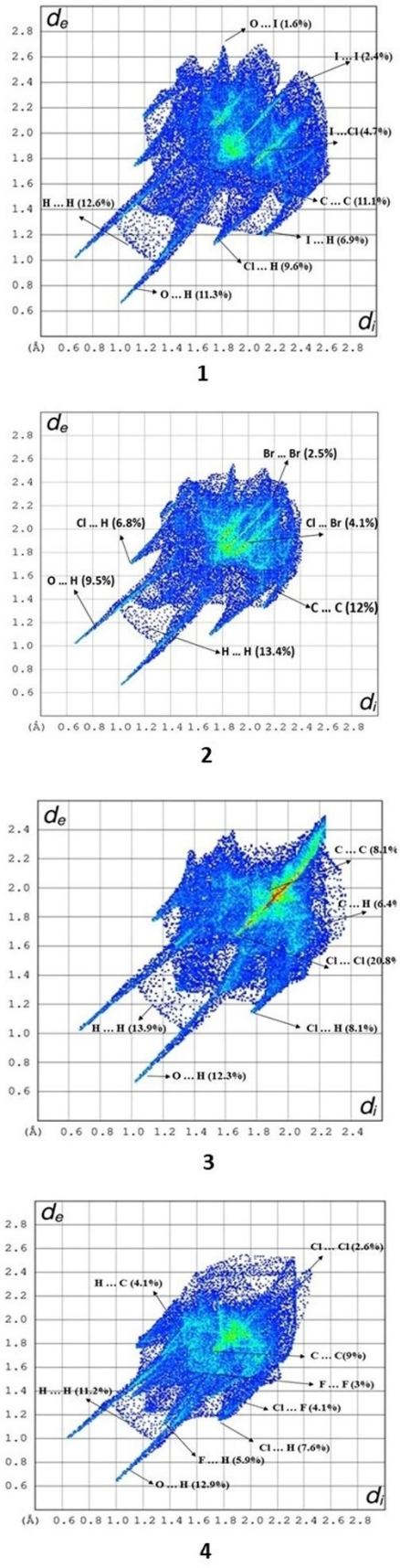

Figure 2. The fingerprint plots with the percentage of contributions to the crystal structure for compounds **1**–**4**.

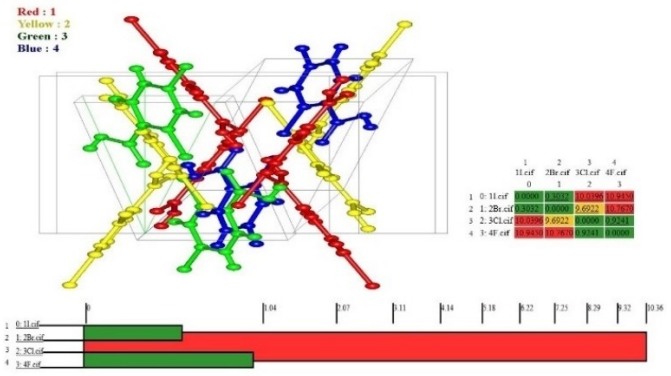

Figure 3. Overlay diagram of unit cell molecules for compounds **1**–**4**. The dendrogram is shown with the packing similarity and dissimilarity values.

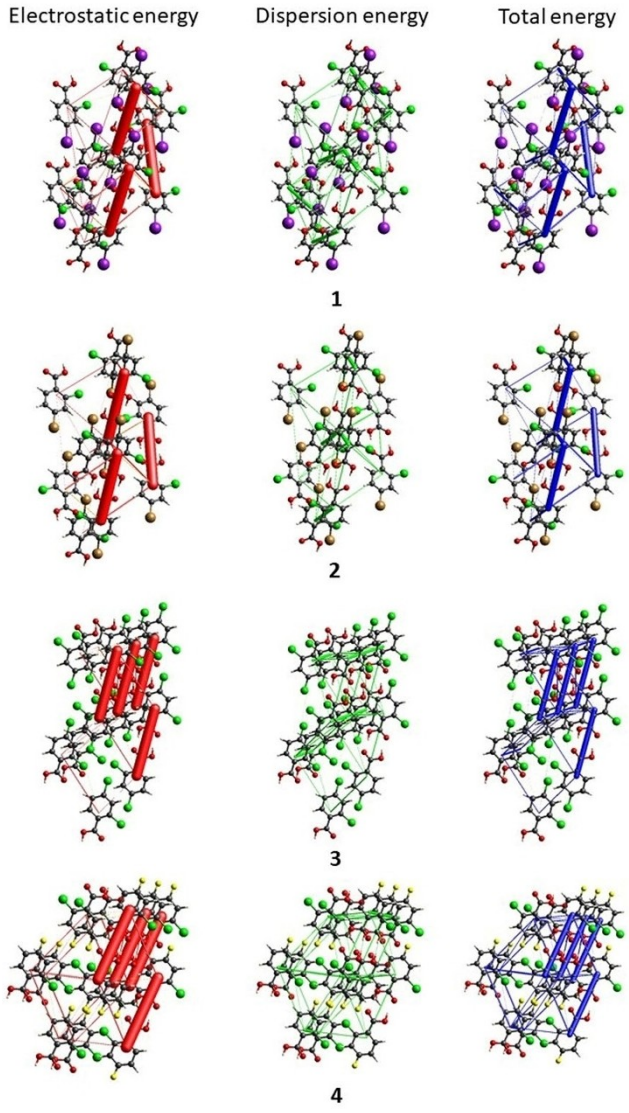

Figure 4. Energy frameworks representing the electrostatic, dispersion and total interaction energy components for the carboxylic acid O–H···O HB dimers in **1**, **2**, **3** and **4**. The tube size is 50 kJmol^{-1} and the energy threshold is zero.

Table 4. Interaction Energies (kJmol^{-1}) obtained from *CrystalExplorer* with the B3LYP/6311G(d,p) functional. R is the distance between molecular centroids in Å.

Interactions	Symmetry	Centroid distance R (Å)	E_{ele}	E_{pol}	E_{dis}	E_{rep}	E_{tot}
1							
I···I	−x+1,−y,−z+2	8.71	−8.1	−0.1	−6.2	11.4	−3.0
I···Cl/ C–H···Cl	−x+1/2, y+1/2, −z+1/2	7.51	−8.2	−0.2	−9.0	8.8	−8.6
O–H···O	−x+2,−y+2,−z+2	11.40	−143.0	−23.2	−11.3	93.1	−84.4
C–H···O	−x+1/2+1,+y−1/2,−z+1/2+1	7.50	−13.7	−1.7	−10.0	9.3	−16.2
C_π···C_π	−x+1,−y+1,−z+2	3.71	−17.2	−0.2	−38.6	27.7	−28.4
C_π···C_π	−x+1,−y+1,−z+2	4.51	−17.7	−0.6	−43.6	25.0	−36.9
I···C_π	−x+1,−y+1,−z+2	9.27	−1.2	−0.2	−5.7	3.0	−4.1
2							
Br···Br	−x+1,−y,−z+2	9.33	−2.9	0.0	−4.4	4.4	−2.8
Br···Cl(1)/ C–H···Cl	−x+1/2,+y−1/2,−z+1/2+2	7.25	−7.0	−0.2	−8.4	7.6	−8.0
Br···Cl(2)	x−1/2,−y−1/2,+z−1/2	7.45	−3.3	−0.1	−5.5	4.8	−4.1
O–H···O	−x+2,−y+2,−z+2	10.23	−138.1	−22.3	−11.3	90.4	−81.4
C–H···O	−x+1/2+1,+y−1/2,−z+1/2+1	7.67	−14.3	−1.9	−7.7	7.7	−16.1
C_π···C_π/ Br···C_π	−x+2,−y+1,−z+2	3.66	−13.4	−0.2	−37.7	22.9	−28.5
C_π···C_π	−x+2,−y+1,−z+2	3.89	−17.7	−0.5	−44.7	25.2	−37.6
3							
Cl···Cl (1)	x,+y+1,+z	11.58	0.0	0.0	−1.0	0.1	−1.0
Cl···Cl (2)/ C–H···O	x+1,+y+1,+z	8.08	−13.4	−0.9	−6.4	10.0	−10.7
O–H···O	−x+2,−y+1,−z+1	8.76	−139.8	−22.6	−11.8	99.6	−74.7
C–H···O	x,+y−1,+z	7.76	1.6	−0.7	−7.8	2.6	−4.4
C–H···Cl	−x, −y, −z	7.13	−7.0	−0.4	−10.6	9.9	−8.1
C_π···C_π	x−1,+y,+z	3.90	−8.6	−0.7	−34.7	18.5	−25.4
4							
F···Cl/ C–H···O/ C–H···Cl	x,+y−1,+z	7.77	−14.0	−1.6	−8.2	8.2	−15.5
		-					
O–H···O	−x+2,−y+1,−z+1	8.04	−139.0	−22.3	−11.5	98.0	−74.8
C–H···F	−x,−y+2,−z+2	8.16	−6.0	−0.3	−7.5	4.3	−9.5
C–H···O	−x+2,−y+2,−z+1	7.37	1.5	−0.8	−10.2	5.4	−4.1
C_π···C_π	x+1,+y,+z	3.82	−7.4	−0.7	−32.7	17.5	−23.4

Type II X···Cl interactions are attractive in nature and their total energy is in the range of weak C–H···O/C–H···Cl HBs. The exact total energy of Type II X···Cl interactions is not available as they are simultaneously associated with other weak HBs namely, C–H···Cl (in **1** and **2**) and C–H···O (in **3** and **4**) HBs. However, the strength of Type I homo-halogen X···X interaction is maximum in the case of iodine and it is gradually decreasing in the order such that I···I (−3.0 kJmol^{-1}) > Br···Br (−2.8 kJmol^{-1}) > Cl···Cl (−1.0 kJmol^{-1}). The total energy is well correlated with the increasing order of polar-flattening effect on halogens and the polarization effect is maximum for iodine. Indeed, the F···F interaction is completely absent in **4**, indicating that the fluorine is not polarized to a larger extend and C–H···F dimers have prevailed over F···F interactions in the crystal structure. Additionally, compounds **3** and **4** have C–H···Cl (−7.9 kJmol^{-1}) and C–H···F (−14.1 kJmol^{-1}) HB dimers, respectively and they have significant contributions to the crystal packing.

Topological properties of electron density

The topological analysis of intermolecular interactions was performed for selected molecular pairs using the *AIMALL* program[46] to understand the nature of non-covalent interactions. The (3,-1) bond critical points (BCPs) are observed for all interactions, which validates the importance of those interactions in the crystal structure. The values interaction length (R_{ij}), electron density (ρ_b) and Laplacian of the electron density ($\nabla^2\rho$), ellipticity (ε), local potential energy (V_b), kinetic energy density (G_b) at BCP are listed in Table 5. The molecular graphs with bond paths and critical points for all intermolecular interactions in **1**–**4** are shown in Figures S3–S7. The small value of ED (ρ_b) and Laplacian ($\nabla^2\rho$) at BCP confirm that all are non-covalent interactions. For all interactions, Laplacian ($\nabla^2\rho$) is found to be positive and $V_b/G_b < 1$ which indicates the closed-shell nature of interactions.[47] The topological properties for the O–H···O HB in the carboxylic acid dimers are larger than all

Table 5. Topological parameters of intermolecular interactions for compounds **1**–**4**. The values reported in the first and second lines correspond to the values from *TOPOND* and *AIMALL*, respectively. The reported experimental values based on the multipole model are shown in italics for compounds **2** and **4**. The G_b and, V_b are kinetic and potential energy densities at BCP in kJmol^{-1} bohr^{-3}, respectively.

Interactions	Distance (Å)	R_{ij} (Å)	ρ_b (eÅ^{-3})	$\nabla^2\rho$ (eÅ^{-5})	ε	G_b	V_b	$\lvert V\rvert/G$	E_{int} (kJ mol^{-1})
1									
I1···I1	3.880	3.895	0.053	0.409	0.11	10.4	−9.2	0.9	−6.3
			0.049	0.506	0.25	11.4	−9.0	0.8	−6.1
I1···Cl1	3.797	3.812	0.040	0.409	0.12	9.3	−7.3	0.8	−5.0
			0.039	0.529	0.23	9.9	−7.0	0.7	−4.8
O2–H2···O1	1.686	1.686	0.229	3.181	0.01	87.8	−88.8	1.0	−44.4
			0.196	3.300	0.04	81.9	−73.8	0.9	−36.9
C5–H5···O1	2.332	2.365	0.053	0.771	0.05	16.3	−11.2	0.7	−5.6
			0.047	0.672	0.04	15.0	−11.8	0.8	−5.9
C3–H3···Cl1	2.919	2.945	0.026	0.361	0.06	7.6	−5.1	0.7	−2.6
			0.037	0.472	0.05	10.1	−7.4	0.5	−3.7
C2···C6	3.576	3.662	0.040	0.409	0.04	9.2	−7.3	0.8	−3.6
(π…π)			0.030	0.299	0.05	7.0	−5.8	0.8	−2.9
I1···C2	3.857	3.961	0.030	0.360	0.05	8.5	−6.2	0.7	−3.1
(I…π)			0.044	0.409	0.06	9.4	−7.7	0.8	−3.9
2									
Br1···Br1	3.699	3.702	0.047	0.409	0.05	9.8	−8.7	0.9	−5.0
			0.034	0.407	0.15	8.8	−6.4	0.7	−3.7
		3.667	*0.056*	*0.536*	*0.02*	*12.3*	*−10.0*	*0.8*	*−5.8*
Br1···Cl1 (1)	3.703	3.715	0.040	0.385	0.09	9.2	−8.0	0.9	−4.6
			0.055	0.385	0.17	8.6	−6.1	0.8	−3.5
		3.613	*0.051*	*0.516*	*0.02*	*9.3*	*−6.9*	*0.8*	*−4.0*
Br1···Cl1 (2)	3.799	3.801	0.034	0.313	0.04	7.6	−6.3	0.8	−3.7
			0.030	0.337	0.06	7.4	−5.3	0.7	−3.1
		3.733	*0.041*	*0.403*	*0.19*	*10.5*	*−8.4*	*0.7*	*−4.9*
O1–H1···O2	1.694	1.698	0.320	3.380	0.01	172.3	−118.3	0.7	−59.1
			0.340	3.020	0.01	169.9	−91.7	0.5	−45.9
		1.646	*0.290*	*5.54*	*0.03*	*139.8*	*−128.7*	*0.9*	*−64.3*
C5–H5···O1	2.275	2.452	0.081	0.451	0.06	16.0	−10.8	0.6	−5.4
			0.079	0.482	0.05	15.8	−9.6	0.6	−6.2
			0.084	0.961	0.03	15.1	−14.2	0.9	−7.1
C3–H3···Cl1	2.802	2.825	0.033	0.516	0.02	12.3	−7.58	0.6	−3.7
			0.047	0.602	0.03	12.9	−9.3	0.7	−4.6
		2.694	*0.058*	*0.744*	*0.02*	*16.2*	*−12.2*	*0.8*	*−6.1*
Br1···C2	3.754	3.795	0.040	0.433	0.83	9.32	−7.2	0.8	−3.5
(Br…π)			0.051	0.467	0.51	10.7	−8.6	0.8	−4.3
3									
Cl1···Cl2	3.342	3.352	0.033	0.385	0.04	8.5	−6.8	0.4	−3.3
			0.032	0.394	0.04	8.1	−5.4	0.7	−2.6
O2–H2···O1	1.682	1.680	0.210	3.084	0.06	79.5	−74.7	0.9	−37.4
			0.310	3.270	0.02	90.5	−92.0	1.0	−46.0
C5–H5···O1	2.986	2.993	0.020	0.241	0.32	5.0	−3.4	0.7	−1.7
			0.021	0.317	0.24	6.6	−4.6	0.7	−2.3
C3–H3···Cl1	3.052	3.062	0.026	0.361	0.39	7.9	−5.7	0.7	−2.9
			0.028	0.336	0.47	6.9	−4.7	0.7	−2.4
C4···C5	3.492	3.606	0.026	0.409	0.50	7.8	−4.3	0.5	−2.1
(π…π)			0.033	0.317	0.47	7.3	−5.9	0.8	−2.9
C1···C2	3.487	3.561	0.026	0.409	0.61	7.7	−4.1	0.5	−2.0
(π…π)			0.034	0.325	0.52	7.4	−6.0	0.8	−3.0
4									
F1···Cl1	3.066	3.032	0.053	0.747	0.01	15.8	−11.3	0.7	−5.5
			0.048	0.847	0.02	18.8	−14.6	0.8	−7.2
		3.021	*0.053*	*0.837*	*0.06*	*16.9*	*−11.1*	*0.7*	*−5.4*
O2–H2···O1	1.676	1.670	0.222	3.181	0.01	82.2	−77.7	0.9	−38.8
			0.325	3.371	0.01	94.6	−97.3	1.0	−48.7
		1.660	*0.277*	*2.790*	*0.00*	*78.0*	*−80.0*	*1.0*	*−40.0*
C5–H5···O1	2.513	2.573	0.033	0.409	0.03	8.8	−6.1	0.7	−3.0
			0.043	0.574	0.03	13.3	−11.0	0.8	−5.5

Table 5. continued

Interactions	Distance (Å)	R_{ij} (Å)	ρ_b (eÅ^{-3})	$\nabla^2\rho$ (eÅ^{-5})	ε	G_b	V_b	$\lvert V\rvert/G$	E_{int} (kJ mol^{-1})
1									
C3–H3···F1	2.506	2.532	0.033	0.506	0.08	10.5	−7.2	0.7	−3.6
			0.043	0.710	0.06	16.0	−12.8	0.8	−6.4
		2.477	*0.026*	*0.502*	*0.41*	*9.6*	*−5.8*	*0.6*	*−2.9*
C6–H6···O2	2.619	2.625	0.033	0.457	0.22	9.3	−6.2	0.7	−3.1
			0.027	0.432	0.19	11.7	−7.0	0.6	−3.5
		2.575	*0.043*	*0.528*	*0.15*	*10.8*	*−7.2*	*0.7*	*−3.6*
C5–H5···O1	2.974	3.012	0.026	0.313	0.13	7.0	−5.2	0.7	−2.6
			0.031	0.397	0.19	8.0	−5.1	0.6	−2.6
C1···C2 (π…π)	3.481	3.521	0.026	0.409	0.68	7.6	−4.0	0.5	−2.0
			0.033	0.305	0.95	6.9	−5.5	0.8	−2.8

the remaining interactions in all compounds. The ρ_b value vary from 0.196 to 0.340 eÅ^{-3} for the O–H···O HB whereas the Laplacian varies in the range from 3.020 to 3.380 eÅ^{-5} (Table 5) which are consistent with literature values of strong O–H···O HBs.[48,49] The interaction energy (E_{int}) obtained from the ED for the O–H···O HB dimers vary in the range from −36.9 to −48.7 kJmol^{-1}. It indicates that the O–H···O HB dimers play a major role in the stabilization of crystal structure. The topological properties obtained for the O–H···O HB dimer from both TOPOND[50] (in the crystal geometry) and AIMALL[46] (in the gas phase) are consistent with the experimental charge density values of compounds **2**[40] and **4**[25] as well as literature values.[48,49] The ρ_b and $\nabla^2\rho$ at BCP for X···Cl and X···X (where X = I, Br, Cl) interactions are in the range 0.032 to 0.053 eÅ^{-3} and 0.313 to 0.529 eÅ^{-5} respectively. The topological properties of C–H···O, C–H···X, C_π··· C_π and X···X interactions show good agreement with literature values[21,23,51] and confirming the non-covalent nature of interactions. The charge depleted (CD) region is facing the charge concentration (CC) region and directly resulting in a δ+··· δ- type of interaction for type II X···X interactions.[52] However, type I X···X interactions are occurring in the crystal packing due to the decreased repulsion from anisotropy of the ED around the halogen atom.[21] The presence of weak C_π··· C_π and X··· C_π (X = I and Br) stacking interacting are confirmed by topological properties at BCP and bond paths connecting the interacting atoms between two adjacent molecules. The topological properties and interaction energies obtained from *TOPOND* and *AIMALL* are comparable with high-resolution experimental multipole models as shown in Table 5 for compounds **2** and **4**. The total energies (E_{int}) have been estimated for all intermolecular interactions using the ρ_b and $\nabla^2\rho$ values at BCP by the Espinosa-Molins-Lecomte (EML) relationship for hydrogen bonds.[53,54] The modified EML relationship as shown by Tsirelson et al.[30] is applied for evaluating the interaction energies of X···X interactions. The E_{int} for O–H···O HB dimers are the highest among all interactions indicating that it is the structure stabilizing interaction in all compounds. However, E_{int} values are underestimated from the topological analysis compared to the energies obtained from the *CrystalExplorer*.[39] Earlier, Spackman had cautioned the use of interaction energies from the EML approach to evaluate the strength of interactions as they may not reflect true energies in the crystalline state.[55] Thus, we are not discussing the hierarchy of interactions based on the EML approach and the discussion on the strength of interactions is solely based on the energies from the *CrystalExplorer* as discussed in the above section.

Molecular Electrostatic Potential maps

The molecular electrostatic potential (MESP) maps were shown for **1**–**4** in the crystal geometry and mapped over the range of −200 kJmol^{-1} (red) to 200 kJmol^{-1} (blue). The deep red color region around the oxygen atom of carboxylic acid shows the negative ESP and the deep blue color region around the hydrogen atom shows the positive ESP (Figure 5). The halogen atoms except fluorine show the positive ESP region (electron-deficient) along with the C–X bond whereas the negative ESP region (electron-rich) is observed perpendicular to the C–X bond. The strength positive ESP region (electron deficient) along the C–X bond is maximum for iodine, which reduces gradually as I > Br > Cl > F. The values V_{max} along with the C–X bond for I, Br, Cl and F are 174, 108, 104, −59 kJmol^{-1},

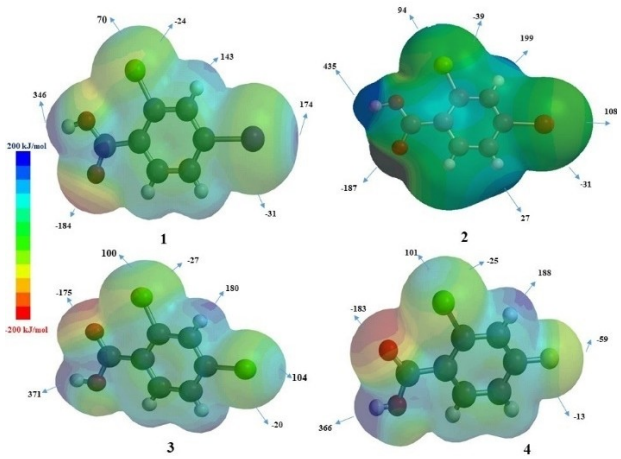

Figure 5. Molecular electrostatic potential (MESP) of **1**–**4** mapped from −200 kJmol^{-1} to 200 kJmol^{-1}.

respectively. The MESP clearly suggests that F do not have any σ-hole along with the C–F bond. This observation is corroborated by the absence of F···F interactions in **4** and C–H···F HB has formed over F···F interactions. This is consistent with earlier studies on the σ-hole formation of halogen atoms. It is interesting to note that the positive ESP region interacts with the negative ESP of the electronegative atoms and the strength of intermolecular interactions are well correlated with observed values of potentials in the MESP map.

Frontier Molecular Orbital (FMO) and Global Reactivity Descriptors

The intramolecular charge transfer from a donor to an acceptor moiety within the molecule is characterized by the excitation of an electron from the highest occupied molecular orbital (HOMO) to the lowest unoccupied molecular orbital (LUMO) and they are named as frontier molecular orbitals.[56] They play an important role in dictating the optical and electric properties of a molecule. The HOMO and LUMO orbitals for compounds **1**–**4** are as shown in Figure 6. The related parameters such as the ionization potential (I) and electron affinity (A), the energy gap (△E), chemical potential (μ), global hardness (η), softness (σ) and electrophilicity index (ω) are listed in Table 6. The HOMO and LUMO in the molecule are mainly localized with large electron density projections on the electrophilicity and electronegativity values.[57] They imply the tendency of the molecules to donate electrons during chemical reactions, thus leading to chemical reactivity.[58] It is observed that compound **4** with fluorine substitution exhibits the lowest energy gap of 5.01 eV among all compounds. Thus, compound **4** is significantly different from other compounds in terms of chemical hardness, electronegativity, chemical reactivity and chemical potential. The FMO parameters for **1**, **2** and **3** are comparable to each other, thus expected to have similar optical and electronic properties (Table 6).

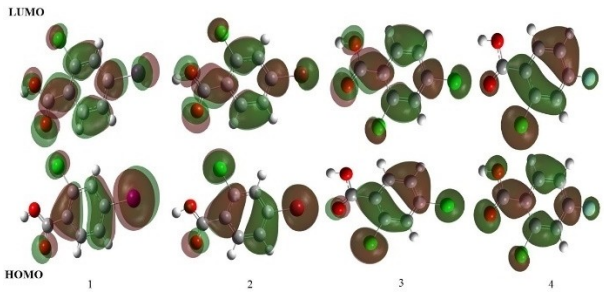

Figure 6. Frontier molecular orbital (FMO) plots for compounds **1**–**4** at isovalue of 0.05 a.u.

Table 6. Calculated FMO parameters for compounds **1**–**4**.

Chemical property	Parameter (eV)	1	2	3	4
HOMO energy	E_H	−7.35	−7.38	−7.48	−7.12
LUMO energy	E_L	−2.09	−2.09	−2.06	−2.11
Energy gap (△ E)	$E_g = E_H.E_L$	5.26	5.29	5.42	5.01
Chemical hardness (η)	$\eta = \lvert E_H\text{-}E_L \rvert /2$	2.63	2.64	2.71	2.51
Softness (ζ)	$\zeta = 1/2\eta$	0.19	0.19	0.18	0.20
Chemical Potential (μ)	$\mu = E_H + E_L/2$	4.72	4.74	4.77	4.61
Electrophilicity index (ω)	$\omega = \mu^2/2\eta$	4.24	4.23	4.20	4.23
Electronegativity (χ)	$\chi = -\mu$	−4.72	−4.74	−4.77	−4.61

Conclusion

The crystal structure of four compounds, 2-Chloro, 4-X-Benzoic Acids (where X = I, Br, Cl and F) have been determined using single crystal X-ray diffraction. The crystal geometry is used for the Hirshfeld surface analysis and subsequent determination of interaction energies in *CrystalExplorer*. Further, the topological properties are determined in both crystal geometry and gas phase using *TOPOND* and *AIMALL*, respectively. The topological properties and interaction energy obtained from the electron density are in good agreement with experimental values, thus validates the present study. The topological properties and bond path confirm these interactions as non-covalent interactions. The topological properties derived from *TOPOND* and *AIMALL* are comparable with the experimental multipolar model values. The interaction energies obtained from the *CrystalExplorer* are used to classify the hierarchy of interactions observed in all compounds. The strength of interactions decreases in the following order such as O–H···O HB dimers > $C_\pi \cdots C_\pi$ aromatic stacking interactions > C–H···O HBs > type II X···Cl interactions and C–H···Cl HBs > type I homo-halogen X···X interactions in all compounds. The energy of carboxylic acid O–H···O HB dimers varies in the range from −74.7 to −84.4 kJmol^{-1} with electrostatic terms (from −139.0 to −143.0 kJmol^{-1}) as a maximum contributor to the total energy. The strength of type I homo-halogen X···X interaction is maximum in the case of iodine and it is gradually decreasing in the order such that I···I (−3.0 kJmol^{-1}) > Br···Br (−2.8 kJmol^{-1}) > Cl···Cl (−1.0 kJmol^{-1}). The type I F···F interaction is absent in **4**, which indicates lower polarizability of the F atom. Further, C–H···F HBs are formed over type I F···F interactions. The decreasing interaction energy for Type I homo-halogen X···X interactions from iodine to fluorine is well correlated with decreasing order of the polar-flattening effect and polarization on halogens. The quantitative insights on HBs and XBs in the molecular compounds are useful in designing new materials based on crystal engineering and supra-molecular principles.

Supporting information summary

Packing diagrams, Hirshfeld surface plots, molecular graphs of compounds and intermolecular interactions, interaction energies from the B3LYP/DGDZVP functional. Deposition Number(s) 2069043 (for **2**), 2069044 (for **3**), 2069045 (for **4**) and 2069046 (for **1**) contain(s) the supplementary crystallographic data for this paper. These data are provided free of charge by the joint Cambridge Crystallographic Data Center and Fachinformationszentrum Karlsruhe Access Strurctures service.

Acknowledgements

The authors are grateful to Professor T. N. Guru Row, Indian Institute of Science for the single crystal X-ray data collection. GNA thanks Vision Group on Science and Technology (VGST), Karnataka, India, for RGS/F grant (VGST/GRD-689/2017-18/2018-19/505). VRH thanks the UGC-India for the financial support under the start-up grant and Faculty Recharge Programme.

Conflict of Interest

The authors declare no conflict of interest.

Data Availability Statement

The data that support the findings of this study are available in the supplementary material of this article.

Keywords: Interaction energy · Halogen bond · Hirshfeld analysis · Hydrogen bond · QTAIM

[1] A. Priimagi, G. Cavallo, P. Metrangolo, G. Resnati, *Acc. Chem. Res.* **2013**, *46*, 2686–2695.
[2] S. K. Seth, D. Sarkar, A. Roy, T. Kar, *CrystEngComm.* **2011**, *13*, 6728–6741.
[3] F. Zordan, L. Brammer, P. Sherwood, *J. Am. Chem. Soc.* **2005**, *127*, 5979–5989.
[4] K. Raatikainen, K. Rissanen, *CrystEngComm.* **2009**, *11*, 750–752.
[5] A. Brown, P. D. Beer, *Chem. Commun.* **2016**, *52*, 8645–8658.
[6] N. K. Noel, A. Abate, S. D. Stranks, E. S. Parrott, V. M. Burlakov, A. Goriely, H. J. Snaith, *ACS Nano.* **2014**, *8*, 9815–9821.
[7] L. Meazza, J. A. Foster, K. Fucke, P. Metrangolo, G. Resnati, J. W. Steed, *Nat. Chem.* **2013**, *5*, 42–47.
[8] A. Abate, M. Saliba, D. J. Hollman, S. D. Stranks, K. Wojciechowski, R. Avolio, G. Grancini, A. Petrozza, H. J. Snaith, *Nano Lett.* **2014**, *14*, 3247–3254.
[9] G. H. L. Mendez, S. Sirimulla, M. Narayan, *Molecules.* **2017**, *22*, 1397.
[10] Y. Lu, Y. Wang, W. Zhu, *Phys. Chem. Chem. Phys.* **2010**, *12*, 4543–4551.
[11] G. Berger, P. Frangville, F. Meyer, *Chem. Commun.* **2020**, *56*, 4970–4981.
[12] G. Cavallo, P. Metrangolo, R. Milani, T. Pilati, A. Priimagi, G. Resnati, G. Terraneo, *Chem. Rev.* **2016**, *116*, 2478–2601.
[13] A. Mukherjee, S. Tothadi, G. R. Desiraju, *Acc. Chem. Res.* **2014**, *47*, 2514–2524.
[14] A. C. Legon, *Phys. Chem. Chem. Phys.* **2010**, *12*, 7736–7747.
[15] G. Berger, J. Soubhye, F. Meyer, *Polym. Chem.* **2015**, *6*, 3559–3580.
[16] M. R. Scholfield, C. M. V. Zanden, M. Carter, P. S. Ho, *Protein Sci.* **2013**, *22*, 139–152.
[17] G. R. Desiraju, P. S. Ho, L. Kloo, A. C. Legon, R. Marquardt, P. Metrangolo, P. Politzer, G. Resnati, K. Rissanen, *Pure Appl. Chem.* **2013**, *85*, 1711–1713.
[18] T. Clark, M. Hennemann, J. S. Murray, P. Politzer, *J. Mol. Model.* **2007**, *13*, 291–296.
[19] P. Politzer, J. S. Murray, T. Clark, *Phys. Chem. Chem. Phys.* **2013**, *15*, 11178–11189.
[20] J. A. R. P. Sarma, G. R. Desiraju, *Acc. Chem. Res.* **1986**, *19*, 222–228.
[21] V. R. Hathwar, T. N. G. Row, *J. Phys. Chem. A.* **2010**, *114*, 13434–13441.
[22] P. Metrangolo, G. Resnati, *IUCrJ.* **2014**, *1*, 5–7.
[23] T. T. T. Bui, S. Dahaoui, C. Lecomte, G. R. Desiraju, E. Espinosa, *Angew. Chem. Int. Ed.* **2009**, *48*, 3838–3841; *Angew. Chem.* **2009**, *121*, 3896–3899.
[24] M. E. Brezgunova, E. Aubert, S. Dahaoui, P. Fertey, S. Lebegue, C. Jelsch, J. G. Angyan, E. Espinosa, *Cryst. Growth Des.* **2012**, *12*, 5373–5386.
[25] V. R. Hathwar, T. N. G. Row, *Cryst. Growth Des.* **2011**, *11*, 1338–1346.
[26] V. A. Karnoukhova, I. V. Fedyanin, K. A. Lyssenko, *Struct. Chem.* **2016**, *27*, 17–24.
[27] C. F. Matta, N. Castillo, R. J. Boyd, *J. Phys. Chem. A.* **2005**, *109*, 3669–3681.
[28] D. Chopra, T. S. Cameron, J. D. Ferrara, T. N. Guru Row, *J. Phys. Chem. A.* **2006**, *110*, 10465–10477.
[29] A. M. S. Riel, R. K. Rowe, E. N. Ho, A.-C. C. Carlsson, A. K. Rappé, O. B. Berryman, P. S. Ho, *Acc. Chem. Res.* **2019**, *52*, 2870–2880.
[30] E. V. Bartashevich, V. G. Tsirelson, *Russ. Chem. Rev.* **2014**, *83*, 1181–1203.
[31] F. Otte, J. Kleinheider, W. Hiller, R. Wang, U. Englert, C. Strohmann, *J. Am. Chem. Soc.* **2021**, *143*, 4133–4137.
[32] G. Ciancaleoni, *Phys. Chem. Chem. Phys.* **2018**, *20*, 8506–8514.
[33] A.-C. C. Carlsson, M. R. Scholfield, R. K. Rowe, M. C. Ford, A. T. Alexander, R. A. Mehl, P. S. Ho, *Biochemistry.* **2018**, *57*, 4135–4147.
[34] R. F. W. Bader, *Atoms in Molecules-A Quantum Theory*, Clarendon, Oxford, **1990**.
[35] C. Gatti, P. Macchi, *Modern Charge Density Analysis*, Springer, New York, **2012**.
[36] V. R. Hathwar, *J. Indian Inst. Sci.* **2017**, *97*, 281–298.
[37] P. Macchi, *Crystallogr. Rev.* **2013**, *19*, 58–101.
[38] M. A. Spackman, D. Jayatilaka *CrystEngComm.* **2009**, *11*, 19–32.
[39] P. R. Spackman, M. J. Turner, J. J. McKinnon, S. K. Wolff, D. J. Grimwood, D. Jayatilaka, M. A. Spackman *J. Appl. Crystallogr.* **2021**, *54*, 1006–1011.
[40] M. S. Pavan, A. K. Jana, S. Natarajan, T. N. Guru Row, *J. Phys. Chem. B.* **2015**, *119*, 11382–11390.
[41] T. Pramanik, M. S. Pavan, T. N. Guru Row, *Faraday Discuss.* **2017**, *203*, 201–212.
[42] A. Rajam, P. T. Muthiah, R. J. Butcher, J. P. Jasinski, J. Wikaira, *Acta Crystallogr. Sect. C* **2018**, *74*, 1007–1019.
[43] R. Ambika, *CSD Communication.* **2017**,It is a data deposition in the CSD. So the journal volume and page numbers are not available.
[44] T. Gelbrich, M. B. Hursthouse, *CrystEngComm.* **2005**, *7*, 324–336.
[45] J. Rohlicek, E. Skorepova, *J. Appl. Crystallogr.* **2020**, *53*, 841–847.
[46] T. A. Keith, *AIMALL*, Version 10.05.04, TK Gristmill Software, **2010**.
[47] C. Gatti, *Z. Kristallogr.* **2005**, *220*, 399–457.
[48] V. R. Hathwar, T. S. Thakur, T. N. G. Row, G. R. Desiraju, *Cryst. Growth Des.* **2011**, *11*, 616–623.
[49] P. Munshi, T. N. G. Row, *CrystEngComm.* **2005**, *7*, 608–611.
[50] C. Gatti, V. R. Saunders, C. Roetti, *J. Chem. Phys.* **1994**, *101*, 10686–10696.
[51] M. V. Vener, A. V. Shishkina, A. A. Rykounov, V. G. Tsirelson, *J. Phys. Chem. A.* **2013**, *117*, 8459–8467.
[52] V. R. Hathwar, R. G. Gonnade, P. Munshi, M. M. Bhadbhade, T. N. G. Row, *Cryst. Growth Des.* **2011**, *11*, 1855–1862.
[53] E. Espinosa, E. Molins, C. Lecomte, *Chem. Phys. Lett.* **1998**, *285*, 170–173.
[54] E. Espinosa, I. Alkorta, J. Elguero, E. Molins, *J. Chem. Phys.* **2002**, *117*, 5529–5542.
[55] M. A. Spackman, *Cryst. Growth Des.* **2015**, *15*, 5624–5628.
[56] R. G. Parr, W. Yang, *J. Am. Chem. Soc.* **1984**, *106*, 4049–4050.
[57] R. G. Parr, L. V. Szentpály, S. Liu, *J. Am. Chem. Soc.* **1999**, *121*, 1922–1924.
[58] A. Sowmya, G. N. A. Kumar, S. Kumar, S. Karki, *ChemistrySelect.* **2021**, *6*, 4265–4272.

Submitted: December 6, 2021
Accepted: January 3, 2022